RSC Advances

PAPER

View Article Online
View Journal | View Issue

Cite this: *RSC Adv.*, 2021, **11**, 37552

Effect of support on hydrogen generation over iron oxides in the chemical looping process

Zhihua Gao, *[a] Fengyan Fu,[a] Lili Niu,[a] Min Jin *[ab] and Xiaohong Wang[a]

Fe_2O_3 is recognized as an excellent oxygen carrier for its low cost and high oxygen capacity. However, pure Fe_2O_3 must be deposited on supports to ensure high reactivity and durability. Here, we proposed several Fe_2O_3-based oxygen carriers using $MgAl_2O_4$, $Ce_{0.8}Gd_{0.2}O_{1.9}$, and $Zr_{0.8}Y_{0.2}O_{1.9}$ as supports and investigated their performance for chemical looping hydrogen generation. The support effect on chemical looping hydrogen generation performance was evaluated, and the fundamental insights were investigated in depth. $Fe_2O_3/Ce_{0.8}Gd_{0.2}O_{1.9}$ exhibited a superior performance regarding high hydrogen yield and stable trend over 20 cycles at 750 °C. However, hydrogen yield of $Fe_2O_3/Zr_{0.8}Y_{0.2}O_{1.9}$ exceeded that of $Fe_2O_3/Ce_{0.8}Gd_{0.2}O_{1.9}$ at higher temperatures (850 °C). Characterizations show that $Ce_{0.8}Gd_{0.2}O_{1.9}$ exhibits the highest oxygen vacancy concentration, which significantly improves the reduction and reoxidation reactions of Fe_2O_3, thus leading to an enhanced hydrogen yield. However, the interaction between Fe_2O_3 and $Ce_{0.8}Gd_{0.2}O_{1.9}$ contributed to the increase in Fe^{2+} concentration, thus decreasing the oxygen capacity during the redox cycle and contributing to the declined hydrogen yield at higher temperatures. This work highlights the potential of $Ce_{0.8}Gd_{0.2}O_{1.9}$ to be used as an effective support for Fe_2O_3 at mid-temperatures. We hope that the support effect in this work can be extended to design and select more active and durable oxygen carriers.

Received 27th September 2021
Accepted 29th October 2021

DOI: 10.1039/d1ra07210b

rsc.li/rsc-advances

Introduction

Fuel cells are promising substitutes for the conventional power generation systems (turbines and engines, *etc.*) since it does not emit CO_2.[1,2] The development of fuel cells has led to hydrogen receiving increasing attention. However, as a secondary energy vector, hydrogen must be generated manually from other energy sources.[3,4]

Nowadays, methane steam reforming (SMR) is the dominant method for hydrogen generation,[5] producing more than 70% of the total hydrogen. However, this method involves complex complicated processes, including multistage water–gas shift, decarburization, and post-hydrogen purification.[6,7] In addition, the need of enormous auxiliary fuel to maintain the strong endothermal reaction would also lead to significant CO_2 emission.[8] In comparison, electrocatalytic water splitting allows hydrogen to be prepared at room temperature and is recognized as a possible method to replace SMR for hydrogen generation.[9] However, this method is kinetically slow and requires precious metals as electrocatalysts to decrease the reaction energy barrier.[10] The low hydrogen generation performance and high cost of the electrocatalysts significantly limit the industrial application of this technique.

In recent years, chemical looping hydrogen generation has drawn a widespread focus and became a strategic frontier in hydrogen production technology.[11] Compared with the SMR process, this technology utilizes metal oxides as redox materials to split the traditional one-step reaction into two consecutive reactions.[12,13] In a typical procedure, oxygen carrier reacts with the reducing agent to release its lattice oxygen in the fuel reactor. After that, the reduced oxygen carrier enters the hydrogen production reactor to react with water vapor to generate hydrogen.[14,15] Pure CO_2 and H_2 are obtained at the exit

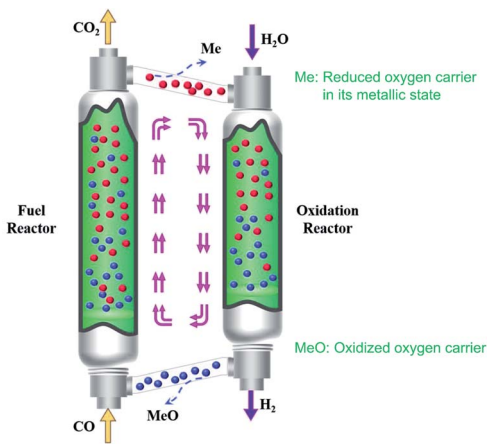

Fig. 1 Scheme of hydrogen generation *via* the chemical looping technology.

[a]*Hengshui University, Department of Applied Chemistry, Heping Road No. 1088, Hengshui 053000, Hebei, P. R. China. E-mail: superman_minjin@163.com; hsxygzhh@163.com*

[b]*Sichuan University, Huanlu Nan No. 21, Chengdu 610041, Sichuan, P. R. China*

of the reduction and hydrogen production reactors. The schematic of this process is illustrated in Fig. 1. Hydrogen generation *via* chemical looping exhibits numerous advantages regarding highly pure hydrogen production,[16] inherent CO_2 separation,[17] feasible to process scale,[18] *etc*. However, the development of highly active and stable oxygen carriers resides in a technical bottleneck for the scale-up of this technology.

Many metal oxides have been proposed and used as oxygen carriers to generate hydrogen, including NiO,[19] CuO,[20] and Fe_2O_3.[21] Fe_2O_3 is recognized as the most prospective candidate among the metal oxides for its low cost,[22] abundance in nature,[23] and environmental compatibility.[24] However, the grains of pure iron oxides tend to aggregate on the surface and contribute to serious sintering in the first few cycles, thus leading to a rapidly deteriorated performance. Although the durability of Fe_2O_3 can be enhanced by limiting the reduction extent of Fe_2O_3 to FeO, the oxidation of Fe to Fe_3O_4 produces nearly four-times the hydrogen compared to FeO to Fe_3O_4. Thus, oxidation from Fe to Fe_3O_4 is more conducive for hydrogen generation.[25] To eliminate the deactivation of pure iron oxides, numerous types of supports were proposed and used to support iron oxides, including, Al_2O_3,[26] TiO_2,[27] $MgAl_2O_4$,[28] and CeO_2.[27] These supports can provide a large specific surface area and function as effective barriers to inhibit iron mitigation and aggregation.[29] Much improved durability was obtained by depositing pure iron oxides on these supports. For example, Rahimpour *et al.*[30] synthesized Fe_2O_3–$MgAl_2O_4$ as an oxygen carrier for hydrogen production and investigated its long-term durability at 700 °C. The durability of Fe_2O_3–$MgAl_2O_4$ significantly improved compared with Fe_2O_3/Al_2O_3 due to the mitigated interaction between Fe_2O_3 and support. Similarly, much improved stability was also obtained by Wang *et al.*[31] using CeO_2 as a support material. By comparing the performance of iron oxide deposited on different supports, the hydrogen production performance varied a lot for iron oxides with different supports, that is, the support properties of oxygen carriers significantly influence the performance of oxygen carriers. However, little work was done to disclose the fundamental of the support effect on the chemical looping hydrogen generation, thus impeding the rational selection and design of suitable oxygen carriers.

In this study, we prepared several Fe_2O_3-based oxygen carriers with various supports ($MgAl_2O_4$, $Ce_{0.8}Gd_{0.2}O_{1.9}$, and $Zr_{0.8}Y_{0.2}O_{1.9}$). The support effect on the chemical looping hydrogen generation was studied, and the fundamental of the support effect was investigated in depth.

Experimental

Material synthesis

A wet-coprecipitation method was employed for the synthesis of the oxygen carriers (Fe_2O_3 : support = 6 : 4). Calculated amount of nitrate precursors was dissolved into deionized water and sufficiently blended to an apparent solution. The temperature of the solution was heated to 70 °C under continuous stirring. After that, the appropriate amount of 26 vol% NH_3 solution was added to keep the pH value at around 9.0. The solution was then aged for 12 h to get the precipitate. The precipitate was filtered, washed for 3 times, and subsequently dried at 120 °C for 4 h. The solid was annealed at 800 °C for 4 h under air. Finally, oxygen carriers were polished and sieved to get the final powder (0.2–0.3 mm) for the experiments. The nominations were termed as Fe_2O_3/CG, Fe_2O_3/ZY, Fe_2O_3/MA for Fe_2O_3/$Ce_{0.8}Gd_{0.2}O_{1.9}$, Fe_2O_3/$Zr_{0.8}Y_{0.2}O_{1.9}$, and Fe_2O_3/$MgAl_2O_4$.

Sample characterizations

The crystallite of the fresh and spent oxygen carriers was investigated by X-ray diffraction (XRD, Rigaku SmartLab) at 40 mA and 44 kV. The patterns were collected between 5° and 80° with the stepwise of 0.05°. Scanning electron microscopy (SEM, JEOL JSM-6010LA) was measured to investigate the oxygen carrier morphologies. The X-ray photoelectron spectroscopy (XPS) measurements were conducted on a Thermo Fisher Scientific Inc. H_2-TPR and CO_2-TPO were carried out on a U-shaped reactor using a mass-spectrometer (OmniStar, Pfeiffer Vacuum) to analyse the outlet gas.

Experimental procedure

A quartz fixed bed was used to conduct the chemical looping hydrogen generation reactions (Fig. 2). 1.0 g oxygen carrier was used for each test. The furnace was heated to the operating temperatures at the ramp rate of 10 °C min^{-1} under Ar atmosphere. The oxygen carriers were then consecutively exposed to 15 vol% CO/Ar and steam/Ar. Ar was employed to sweep the residue gases between the reduction and reoxidation reactions. The off-gas was condensed and then dried by silica gel before entering the gas analyzer. The durability of oxygen carriers was evaluated by performing chemical looping redox cycles for 20 times. Fresh samples were used to evaluate the durability of oxygen carriers at different temperatures.

Results and discussion

Characterizations of oxygen carriers

Fig. 3 displays the XRD of the Fe_2O_3-based oxygen carriers with various supports. Clearly, the characteristic peaks at around 24.12°, 33.12°, 35.61°, 40.82°, 49.42°, 54.0°, and 57.51° fit well with (012), (104), (110), (113), (024), (116), and (018) planes of the Fe_2O_3 phase (PDF 97-001-5840), respectively. For Fe_2O_3/

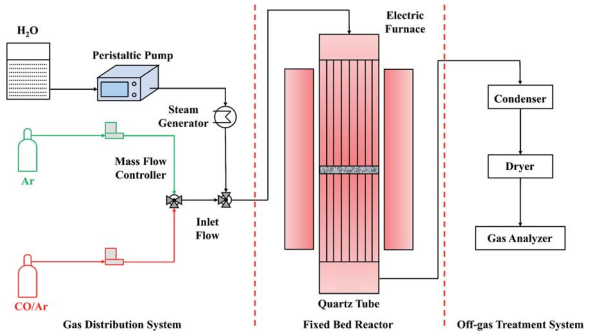

Fig. 2 Schematic of the experimental setup.

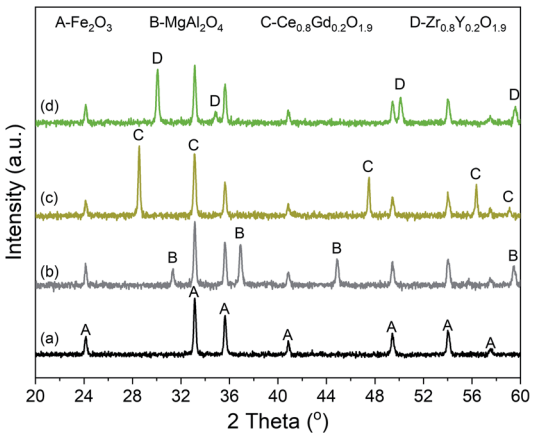

Fig. 3 XRD patterns of the oxygen carriers. (a) Fe_2O_3, (b) Fe_2O_3/MA, (c) Fe_2O_3/CG, and (d) Fe_2O_3/ZY.

$MgAl_2O_4$, additional peaks corresponded well with the spinel structured $MgAl_2O_4$ phase (PDF 97-002-4766), while no peaks for Al_2O_3 or MgO can be observed. Similarly, peaks for $Ce_{0.8}Gd_{0.2}O_{1.9}$ can be found for Fe_2O_3/CG, and reflections for $Zr_{0.8}Y_{0.2}O_{1.9}$ are observed for Fe_2O_3/ZY. These results indicate the successful deposition of Fe_2O_3 on the support materials. The influence of the support materials on the oxygen vacancy concentration was investigated by deconvoluting the O 1s XPS spectrum (Fig. 4). We can observe three peaks at around ~529.5, 531.5 and 533.0 eV, which are labelled as O_I, O_{II}, and O_{III}, respectively. In addition, these peaks can correspond to the lattice oxygen (O_I), oxygen vacancy (O_{II}), and absorbed oxygen (O_{III}), respectively.[32] Table 1 shows the O species concentration of the oxygen carriers. We can observe from the results that the oxygen vacancy concentration of the oxygen carriers can be ranked as: Fe_2O_3/CG > Fe_2O_3/ZY > Fe_2O_3/MA > Fe_2O_3. Specifically, the oxygen vacancy concentration for Fe_2O_3/CG is 19.1%, which is almost twice as large as that of Fe_2O_3. Since the presence of oxygen vacancies can significantly promote lattice oxygen diffusion, which is the rate-determining step of the chemical looping processes,[33] oxygen carriers with higher oxygen vacancy concentration hold the promise to be more reactive during the chemical looping processes. The interaction between Fe_2O_3 and the support materials were characterized by the Fe 2p spectrum. The peaks corresponding to Fe^{2+} $2p_{3/2}$, Fe^{3+} $2p_{3/2}$, satellite, Fe^{3+} $2p_{1/2}$, Fe^{2+} $2p_{1/2}$ are marked in Fig. 5. The corresponding Fe species content can be observed in Table 1. By comparing the Fe^{2+} concentration of the oxygen carriers, Fe_2O_3/CG showed the highest Fe^{2+} concentration of 38.7% among the four oxygen carriers. The remaining oxygen carriers show similar Fe^{2+} concentration at around 30%. These results indicated that a part of Fe dissolved into the lattice of $Ce_{0.8}Gd_{0.2}O_{1.9}$, and the Fe species dissolved into the support lattice for Fe_2O_3/MA and Fe_2O_3/ZY were negligible. Fig. 6 shows the SEM of the fresh oxygen carriers. It can be seen that similar porous structures composed of grains with the size ranging from 50–200 nm can be observed for the fresh samples.

Table 1 The surface species concentration of the oxygen carriers

Sample	O species concentration (%)			Fe species concentration (%)	
	O_I	O_{II}	O_{III}	Fe^{2+}	Fe^{3+}
Fe_2O_3	61.3	10.7	28.0	29.1	70.9
Fe_2O_3/MA	60.0	12.2	27.8	29.8	70.2
Fe_2O_3/CG	57.6	19.1	23.3	38.7	61.3
Fe_2O_3/ZY	59.0	15.8	25.2	30.8	69.2

Redox performance evaluation

The influence of supports on the hydrogen production performance was investigated regarding hydrogen productivity and long-term stability. Fig. 7 shows the temperature-dependent hydrogen yield of the oxygen carriers with different supports.

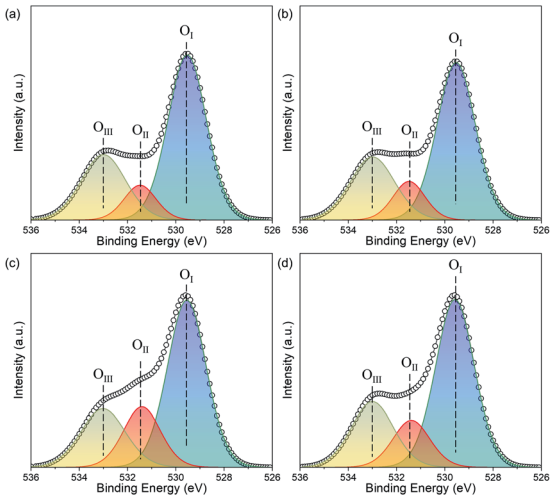

Fig. 4 O 1s spectrum of the as-synthesized oxygen carriers. (a) Fe_2O_3, (b) Fe_2O_3/MA, (c) Fe_2O_3/CG, and (d) Fe_2O_3/ZY.

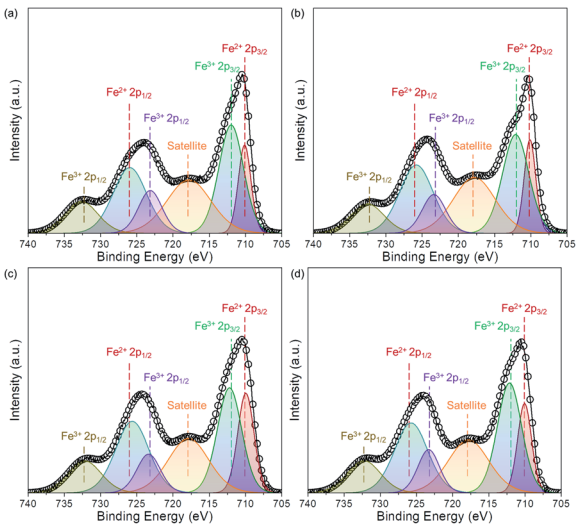

Fig. 5 Fe 2p spectrum of the as-synthesized oxygen carriers. (a) Fe_2O_3, (b) Fe_2O_3/MA, (c) Fe_2O_3/CG, and (d) Fe_2O_3/ZY.

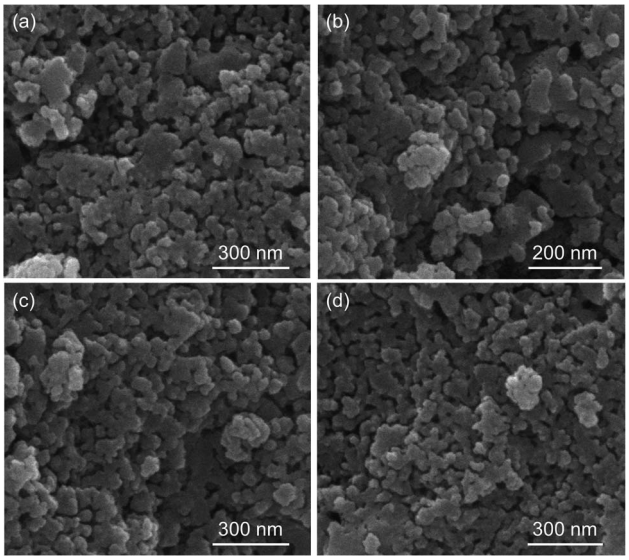

Fig. 6 SEM of the proposed samples. (a) Fe_2O_3, (b) Fe_2O_3/MA, (c) Fe_2O_3/CG, and (d) Fe_2O_3/ZY.

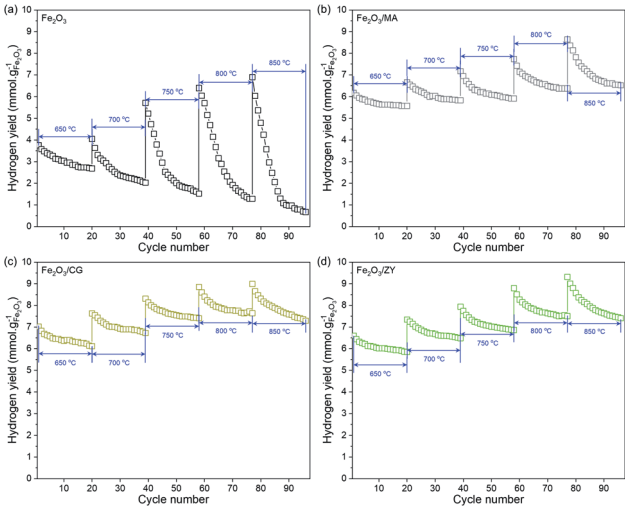

Fig. 8 Effect of the temperature on the durability of oxygen carriers with different supports.

The hydrogen yield tends to rise with the increase in the operating temperature. Depositing Fe_2O_3 on the supports significantly improved the hydrogen productivity. The hydrogen yield at moderate temperatures (<750 °C) followed the sequence: Fe_2O_3/CG > Fe_2O_3/ZY > Fe_2O_3/MA > Fe_2O_3. Comparing hydrogen yields of Fe_2O_3/CG and Fe_2O_3/ZY, we can find that the hydrogen yield of Fe_2O_3/CG exceeded that of Fe_2O_3/ZY at temperatures lower than 750 °C. However, the difference between the hydrogen yield declined with the temperature increase. The hydrogen yield of Fe_2O_3/ZY exceeded that of Fe_2O_3/CG at temperatures > 800 °C.

The influence of the support on the durability was studied by operating the chemical looping hydrogen generation reactions for 20 cycles at the temperature range of 650–850 °C. It can be seen in Fig. 8(a) that a sharp decline in hydrogen production performance can be observed for pure Fe_2O_3 in the temperature range of 650–850 °C. Furthermore, increasing the operating temperature could enhance the deterioration of the hydrogen production performance. The hydrogen yield over 20 redox cycles decreased by 28.5% and 90.3% for pure Fe_2O_3 at 650 °C and 850 °C, respectively. As shown in Fig. 8(b–d), the supported Fe_2O_3 exhibited much mitigated decline in hydrogen productivity after 20 cycles, particularly at lower temperatures. It is also interesting to point out that Fe_2O_3/CG and Fe_2O_3/ZY displayed a more stable trend than Fe_2O_3/MA at 850 °C. The decrease in hydrogen yield after 20 cycles did not exceed 25% even for Fe_2O_3/MA at 850 °C. We can conclude from the results that depositing Fe_2O_3 on the support significantly improved the durability of iron oxides. Among the four oxygen carriers, Fe_2O_3/CG was more suitable to be operated at temperatures < 750 °C, and Fe_2O_3/ZY can be used at higher temperatures. The fundamental mechanism for the support effect on the hydrogen production performance was investigated in depth in the following sections.

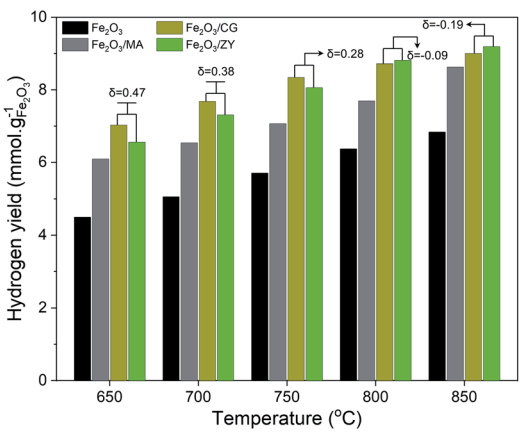

Fig. 7 Hydrogen productivity of the samples at the temperature range of 650–850 °C.

Effect of support on the redox reactions

The support effect on the reductivity is shown in Fig. 9(a). Pure Fe_2O_3 exhibited two distinct peaks with a narrow peak at ~450 °C and a broad peak at the temperature range of 500–900 °C. The two peaks could be explained by the stepwise reduction of Fe_2O_3. The peak at ~450 °C corresponds to the reduction of Fe_2O_3 to Fe_3O_4. The broad peak at higher temperatures can be ascribed to the reduction of Fe_3O_4 to FeO and subsequently to Fe. It can also be seen from the TPR profile that the full reduction of Fe_2O_3 was not achieved even at 900 °C. After depositing Fe_2O_3 on support materials, the reduction peaks shifted to lower temperatures. The reduction temperature of the supported Fe_2O_3 could be ranked as: Fe_2O_3/MA > Fe_2O_3/ZY > Fe_2O_3/CG. These results implied that depositing Fe_2O_3 on the support materials significantly improved the reductivity of Fe_2O_3, and Fe_2O_3/CG showed the best reductivity at both low and moderate temperatures. Since the hydrogen yield is significantly influenced by the reduction depth. The enhanced reductivity of Fe_2O_3/CG can be used to explain its high hydrogen

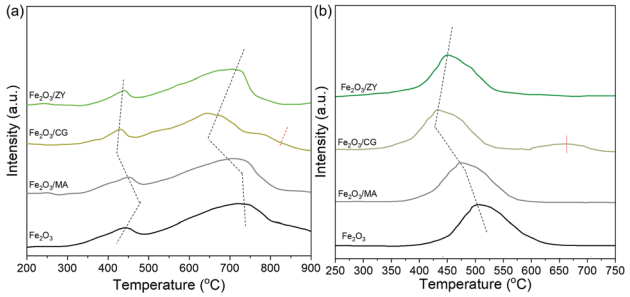

Fig. 9 (a) H_2-TPR, and (b) CO_2-TPD profiles of the fresh oxygen carrier.

yield at moderate temperatures (<750 °C). It is also worth noting that an obvious peak can also be observed for Fe_2O_3/CG at around 800 °C. However, this peak cannot be observed for Fe_2O_3/MA and Fe_2O_3/ZY. Thus, the presence of the peak at higher temperatures indicated that the reduction mechanism differed for Fe_2O_3/CG with Fe_2O_3/MA and Fe_2O_3/ZY. The relatively lower hydrogen yield of Fe_2O_3/CG can also be attributed to the presence of this peak. Similarly, the reoxidation reactivity of oxygen carriers was investigated by CO_2-TPO shown in Fig. 9(b). We could observe from the results that Fe_2O_3/CG exhibited the best reoxidation reaction at mid-temperatures. The presence of the peak at higher temperatures could be explained by the reoxidation of the unreactive $FeCeGdO_x$ solid solution.

Effect of support on phase evolutions and morphologies

H_2-TPR profiles have manifested that depositing Fe_2O_3 on supports can enhance the reductivity and the reduction may differ for Fe_2O_3/CG at higher temperatures. The phase evolution of the reduced samples was evaluated by conducting XRD on the reduced oxygen carriers to disclose the fundamental of the support effect on the reduction reaction.

Fig. 10(a) displays the XRD patterns of the oxygen carriers after being reduced at 650 °C for 25 min. It can be seen that Fe_2O_3 exhibited peaks corresponding to the phases of Fe_3O_4, FeO, and Fe. No peaks for Fe_2O_3 can be observed, indicating that all Fe_2O_3 was reduced to its lower valence state. Depositing Fe_2O_3 on the support materials improved the metallic Fe content in all Fe species, which was evidenced by the intensity of peaks for Fe species. An increase in the Fe content implied that the support materials promoted the reduction depth, which was in line with the H_2-TPR results (Fig. 9). In addition, Fe_2O_3/CG showed the most metallic Fe among the three supported oxygen carriers at 650 °C. The relatively high reduction depth for Fe_2O_3/CG can be used to explain its high hydrogen yield at moderate temperatures. Comparing the XRD patterns of the reduced oxygen carriers, it is obvious that characteristic peaks for $Fe_xCe_{2-x}O_3$ appeared for Fe_2O_3/CG, implying that a part of iron oxide reacts with $Ce_{0.8}Gd_{0.2}O_{1.9}$ to form a solid solution. No reaction between iron oxides and support could be evidenced for Fe_2O_3/MA and Fe_2O_3/ZY. The XRD patterns of the oxygen carriers reduced at 850 °C can be found in Fig. 10(b). The increase in the reduction temperature improved the reduction depth of all oxygen carriers. Almost all iron oxides were reduced

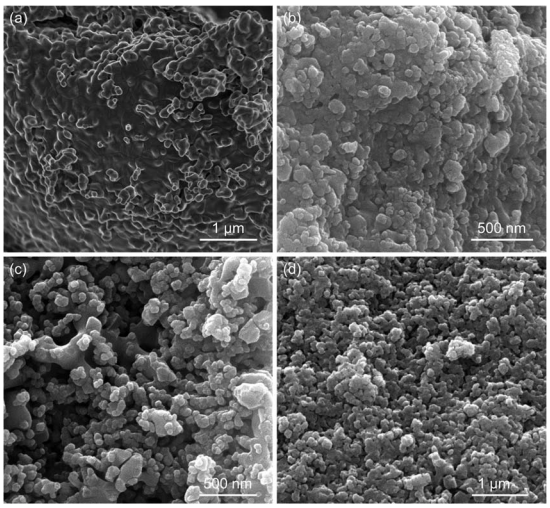

Fig. 11 SEM images of the oxygen carriers after 20 cycles at 750 °C. (a) Fe_2O_3, (b) Fe_2O_3/MA, (c) Fe_2O_3/CG, and (d) Fe_2O_3/ZY.

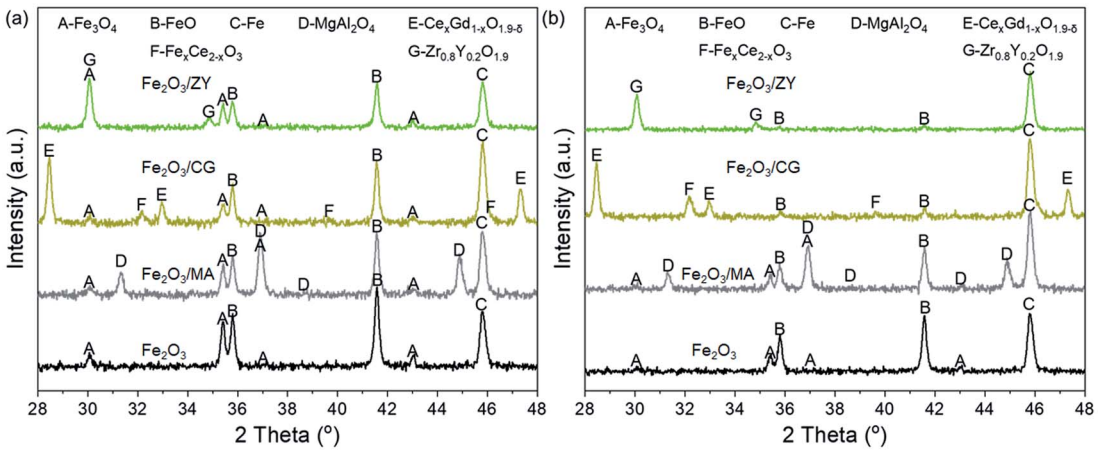

Fig. 10 XRD patterns of the oxygen carriers after reduction at (a) 650 °C and (b) 850 °C for 25 min.

to its metallic state for Fe_2O_3/ZY, while a part of iron oxide was still in the state of $Fe_xCe_{2-x}O_3$ for Fe_2O_3/CG. Thus, the relatively lower hydrogen yield of Fe_2O_3/CG than Fe_2O_3/ZY can be explained by the formation of $Fe_xCe_{2-x}O_3$ to decrease the oxygen capacity of Fe_2O_3/CG. Fig. 11 shows the SEM of the spent oxygen carriers at 750 °C. It can be seen that serious sintering of Fe_2O_3 could be observed by the agglomerated small grains, which severely blocks the pores and limits the diffusion of the reactant gas. The deteriorated performance during 20 cycles was consistent with the severely sintered particles of the oxygen carrier. Also, obvious particle magnification can be observed for the supported Fe_2O_3. However, the pores still existed for these oxygen carriers, and these oxygen carriers exhibited negligible grain agglomeration compared with pure Fe_2O_3. This phenomenon is attributed to the interactions between the support materials with the reduced Fe species.

Conclusions

In this study, we synthesized three Fe_2O_3-based oxygen carriers supported by $MgAl_2O_4$, $Ce_{0.8}Gd_{0.2}O_{1.9}$, and $Zr_{0.8}Y_{0.2}O_{1.9}$. The chemical looping hydrogen generation performance regarding hydrogen yield and durability at 650–850 °C was investigated. Fe_2O_3/CG displayed high hydrogen yield and superior durability at mid-temperatures (<800 °C). Characterizations manifested that depositing Fe_2O_3 on $Ce_{0.8}Gd_{0.2}O_{1.9}$ improved the oxygen vacancy concentration. The high oxygen vacancy concentration was beneficial to the reduction and reoxidation reactions of oxygen carriers, thus contributing to a superior hydrogen yield at temperatures below 800 °C. However, the solid reaction between Fe_2O_3 and $Ce_{0.8}Gd_{0.2}O_{1.9}$ contributed to the formation of $Fe_xCe_{2-x}O_3$, which decreased the oxygen capacity of oxygen carriers, particularly at higher temperatures. The decreased oxygen capacity can be used to explain the relatively lower hydrogen yield of Fe_2O_3/CG than that of Fe_2O_3/ZY at 850 °C. The enhanced durability of the supported iron oxides attributed to the mitigated aggregation of grains on the surface. The support effect in this work can be extended to develop and select suitable oxygen carriers for other applications.

Conflicts of interest

There are no conflicts to declare.

Acknowledgements

This work is financially supported by the Key R&D Project of Hebei Province 18214321, the Research Foundation of Hengshui University for High-level Talents 2019GC10 and 2021GC06, the National Innovation and Entrepreneurship Training Program for College Students 202010101001 and 2018011002Z the Science Technology Program of Hengshui City.

References

1 M. Schumann, C. Cosse, D. Becker, D. Vorwerk and D. Schulz, *Int. J. Hydrogen Energy*, 2021, **46**, 28734–28747.
2 F. R. García-García, Y. H. Ma, I. Rodríguez-Ramos and A. Guerrero-Ruiz, *Catal. Commun.*, 2008, **9**, 482–486.
3 A. Ajanovic and R. Haas, *Int. J. Hydrogen Energy*, 2021, **46**, 10049–10058.
4 W. Liu, L. Li, S. Lin, Y. Luo, Z. Bao, Y. Mao, K. Li, D. Wu and H. Peng, *J. Energy Chem.*, 2022, **65**, 34–47.
5 X. Chu, X. Zeng, T. Zheng, W. Zhuang, Y. Yang, W. Zhou and Y. Hong, *Int. J. Hydrogen Energy*, 2020, **45**, 20859–20874.
6 A. M. Ranjekar and G. D. Yadav, *Ind. Eng. Chem. Res.*, 2021, **60**, 89–113.
7 M. Varmazyari, Y. Khani, F. Bahadoran, Z. Shariatinia and S. Soltanali, *Int. J. Hydrogen Energy*, 2021, **46**, 565–580.
8 Y. Wang, D. Liang, C. Wang, M. Chen, Z. Tang, J. Hu, Z. Yang, H. Zhang, J. Wang and S. Liu, *Renewable Energy*, 2020, **160**, 597–611.
9 B. You, M. T. Tang, C. Tsai, F. Abild-Pedersen, X. Zheng and H. Li, *Adv. Mater.*, 2019, **31**, 1807001.
10 C. Acar and I. Dincer, *J. Cleaner Prod.*, 2019, **218**, 835–849.
11 S. Ma, S. Chen, H. Ge, T. Song, P. Lu and W. Xiang, *Energy Fuels*, 2020, **34**, 10256–10267.
12 X. Zhang, Y. Su, C. Pei, Z.-J. Zhao, R. Liu and J. Gong, *Chem. Eng. Sci.*, 2020, **223**, 115707.
13 A. Mishra and F. Li, *Curr. Opin. Chem. Eng.*, 2018, **20**, 143–150.
14 X. Zhao, H. Zhou, V. S. Sikarwar, M. Zhao, A.-H. A. Park, P. S. Fennell, L. Shen and L.-S. Fan, *Energy Environ. Sci.*, 2017, **10**, 1885–1910.
15 Y. Qiu, L. Ma, M. Li, D. Cui, S. Zhang, D. Zeng and R. Xiao, *Chem. Eng. J.*, 2020, **387**, 124150.
16 O. Oruc and I. Dincer, *Int. J. Hydrogen Energy*, 2020, **45**, 34557–34565.
17 Q. Jiang, H. Zhang, Y. Cao, H. Hong and H. Jin, *Energy Convers. Manage.*, 2019, **187**, 523–536.
18 G. Li, Y. Chang, T. Liu, Z. Yu, Z. Liu, F. Liu, S. Ma, Y. Weng and Y. Zhang, *Energy*, 2020, **206**, 118243.
19 Y. Ni, C. Wang, Y. Chen, X. Cai, B. Dou, H. Chen, Y. Xu, B. Jiang and K. Wang, *Appl. Therm. Eng.*, 2017, **124**, 454–465.
20 L. Tan, C. Qin, Z. Zhang, J. Ran and V. Manovic, *Energy Technol.*, 2018, **6**, 1777–1787.
21 Y. Feng, N. Wang, X. Guo and S. Zhang, *Fuel*, 2020, **262**, 116489.
22 T. Liu, Z. Yu, G. Li, S. Guo, J. Shan, C. Li and Y. Fang, *Int. J. Hydrogen Energy*, 2018, **43**, 19384–19395.
23 S. Ma, M. Li, G. Wang, L. Zhang, S. Chen, Z. Sun, J. Hu, M. Zhu and W. Xiang, *Chem. Eng. J.*, 2018, **346**, 712–725.
24 Q. Hu, Y. Shen, J. W. Chew, T. Ge and C.-H. Wang, *Chem. Eng. J.*, 2020, **379**, 122346.
25 Z. Sun, S. Chen, J. Hu, A. Chen, A. H. Rony, C. K. Russell, W. Xiang, M. Fan, M. Darby Dyar and E. C. Dklute, *Appl. Energy*, 2018, **211**, 431–442.
26 S. Zhang, Y. Feng and X. Guo, *Energy Fuels*, 2021, **35**, 626–635.
27 Y. Feng, N. Wang, X. Guo and S. Zhang, *Fuel*, 2020, **276**, 117942.
28 D.-W. Zeng, S. Peng, C. Chen, J.-M. Zeng, S. Zhang, H.-Y. Zhang and R. Xiao, *Int. J. Hydrogen Energy*, 2016, **41**, 22711–22721.

29 D. Zeng, Y. Qiu, M. Li, L. Ma, D. Cui, S. Zhang and R. Xiao, *Appl. Catal., B*, 2021, **281**, 119472.
30 A. Hafizi and M. R. Rahimpour, *Catalysts*, 2018, **8**, 27.
31 X. Zhu, M. Zhang, K. Li, Y. Wei, Y. Zheng, J. Hu and H. Wang, *Chem. Eng. Sci.*, 2018, **179**, 92–103.
32 X. Zhu, K. Li, Y. Wei, H. Wang and L. Sun, *Energy Fuels*, 2014, **28**, 754–760.
33 F. Li, S. Luo, Z. Sun, X. Bao and L.-S. Fan, *Energy Environ. Sci.*, 2011, **4**, 3661–3667.